Pergamon

Geochimica et Cosmochimica Acta, Vol. 67, No. 3, pp. 529–541, 2003

0016-7037/03 $22.00 + .00

PII S0016-7037(02)01091-8

The influence of cosmic-ray production on extinct nuclide systems

INGO LEYA,*[,1] RAINER WIELER, and ALEX. N. HALLIDAY
ETH Zürich, Isotope Geology and Mineral Resources, NO C61, 8092 Zürich, Switzerland

(*Received October* 8, 2001; *accepted in revised form May* 30, 2002)

Abstract—Variations in the atomic abundances of ^{53}Cr, ^{92}Zr, ^{98}Ru, ^{99}Ru, and ^{182}W in meteorites and lunar samples relative to terrestrial values may imply the early decay of radioactive ^{53}Mn, ^{92}Nb, ^{98}Tc, ^{99}Tc and ^{182}Hf, respectively. From this one can deduce nucleosynthetic sites and early solar system timescales. Because these effects are very small, production and consumption of the respective isotopes by cosmic-ray interactions is a concern. It has recently been demonstrated that ^{182}W production by neutron capture reactions on ^{181}Ta is crucial for most lunar samples (Leya et al., 2000a). In this study the neutron fluence of each sample was estimated from its nominal cosmic-ray exposure age as deduced from noble gas data. This approach overestimates the true cosmogenic isotopic shift for samples that might have been irradiated very close to the regolith surface. Here we therefore combine our model calculations with the neutron dose proxies ^{157}Gd/^{158}Gd and ^{149}Sm/^{150}Sm. This allows us to accurately correct the measured W isotopic data for cosmic-ray induced shifts without the explicit knowledge of the exposure age or the shielding depth of the sample simply by measuring ^{157}Gd/^{158}Gd and/or ^{149}Sm/^{150}Sm in an aliquot. In addition we present new model results for the GCR-induced effects on ^{53}Mn-^{53}Cr, ^{92}Nb-^{92}Zr and ^{98}Tc-^{99}Tc-^{98}Ru-^{99}Ru. For each of these systems, except Tc-Ru, a proper cosmic-ray dose proxy is given, permitting the accurate correction of measured isotopic ratios for cosmogenic contributions.

1. INTRODUCTION

The abundances of the daughter products of short-lived nuclides in meteorites and lunar rocks are widely used to decipher early solar system processes. For example, ^{182}Hf-^{182}W, ^{53}Mn-^{53}Cr, ^{92}Nb-^{92}Zr, ^{98}Tc-^{98}Ru, and ^{99}Tc-^{99}Ru have been used to deduce the formation age of the first solids in the solar nebula, the age of the Earth's core, the formation interval of asteroidal cores, the accretion rate of the Earth, the rate of accretion and metal segregation in Mars and various meteorite parent bodies and the formation interval of various early minerals. The excesses of the daughter products typically are on the order of a few ε-units only, where 1 ε is the deviation in parts/10^4 from some standard value. Therefore, cosmic-ray induced production and consumption of the daughter isotopes as well as those used to correct for instrumental mass fractionation need to be assessed, especially for samples exposed for a long time to the galactic cosmic radiation (GCR). In a recent publication we demonstrated that GCR-induced effects in lunar samples can explain the entire measured W isotopic anomaly in some samples (Leya et al., 2000a). These model predictions have been confirmed experimentally. For four lunar mare basalts, the observed correlations between ^{182}W/^{184}W and the Ta/W ratios in mineral separates agree to within ±40% with the model predictions for a cosmogenic contribution (Lee et al., 2001). However, the equations given in that paper to correct for GCR-induced W isotopic shifts suffer from the lack of a reliable neutron dose proxy (Leya et al., 2000a). In that first study we determined the dose of thermal and epithermal neutrons via the ^{21}Ne and ^{38}Ar cosmic-ray exposure ages because such data are widely available. While this approach is quite reliable for shielding depths larger than ~200 g/cm^2, it overestimates GCR-induced effects by up to a factor of 10 for samples which were irradiated at the very top of the lunar regolith (Leya et al., 2000a; 2001a), because the flux of thermal and epithermal neutrons builds up slower than those for medium to high energetic spallation projectiles. This can be improved by using ratios such as ^{149}Sm/^{150}Sm and ^{157}Gd/^{158}Gd as proxies for the fluences of slow neutrons. First results of this approach have been given by Leya et al. (2001a), who also present preliminary estimates for the GCR-induced effects on the ^{53}Mn-^{53}Cr and ^{92}Nb-^{92}Zr systems in meteorites and lunar rocks. Here we will present a comprehensive study of the GCR-induced effects on the extinct nuclide systems ^{182}Hf-^{182}W, ^{92}Nb-^{92}Zr, ^{53}Mn-^{53}Cr, ^{98}Tc-^{98}Ru and ^{99}Tc-^{99}Ru for stony and iron meteorites as well as for lunar rocks. For the first three of these systems, we present a proper measure of the incident particle fluence (^{149}Sm/^{150}Sm, ^{157}Gd/^{158}Gd, and ^{54}Cr/^{52}Cr, respectively). Note that we cover here only the extinct nuclide systems that have not been studied so far for GCR-induced effects, e.g., Goswami (1998). Thus, the light nuclide systems, e.g., ^{10}Be-^{10}B, ^{26}Al-^{26}Mg, and ^{41}Ca-^{41}K, are not included here. We also do not investigate the system ^{107}Pd-^{108}Ag in iron meteorites, for which Reedy (1980) already showed cosmogenic effects to be negligible.

Besides isotopic anomalies connected to radioactive decay of now extinct nuclides ('radiogenic') there exist also non-radiogenic isotope anomalies, as in the Cr-isotopic composition of the CI chondrite Orgueil (Podosek et al., 1997). However, here we concentrate on the effects on radiogenic systems. The ^{182}Hf-^{182}W-system (half-life ^{182}Hf = 9 × 10^6 a) is discussed by Harper et al. (1991) and Halliday et al. (1996), the ^{53}Mn-^{53}Cr-system (half-life ^{53}Mn = 3.7 × 10^6 a) by Birck and Allègre (1988) and Lugmair and Shukolyukov (1998) and the ^{92}Nb-^{92}Zr system (half-life ^{92}Nb = 36 × 10^6 a) by Harper (1996). For the ^{98}Tc-^{99}Tc-^{98}Ru-^{99}Ru system (half-life ^{98}Tc = 4.2 × 10^6 a, ^{99}Tc = 0.21 × 10^6 a) see Poths et al. (1987) and

* Author to whom correspondence should be addressed (Leya@erdw.ethz.ch).

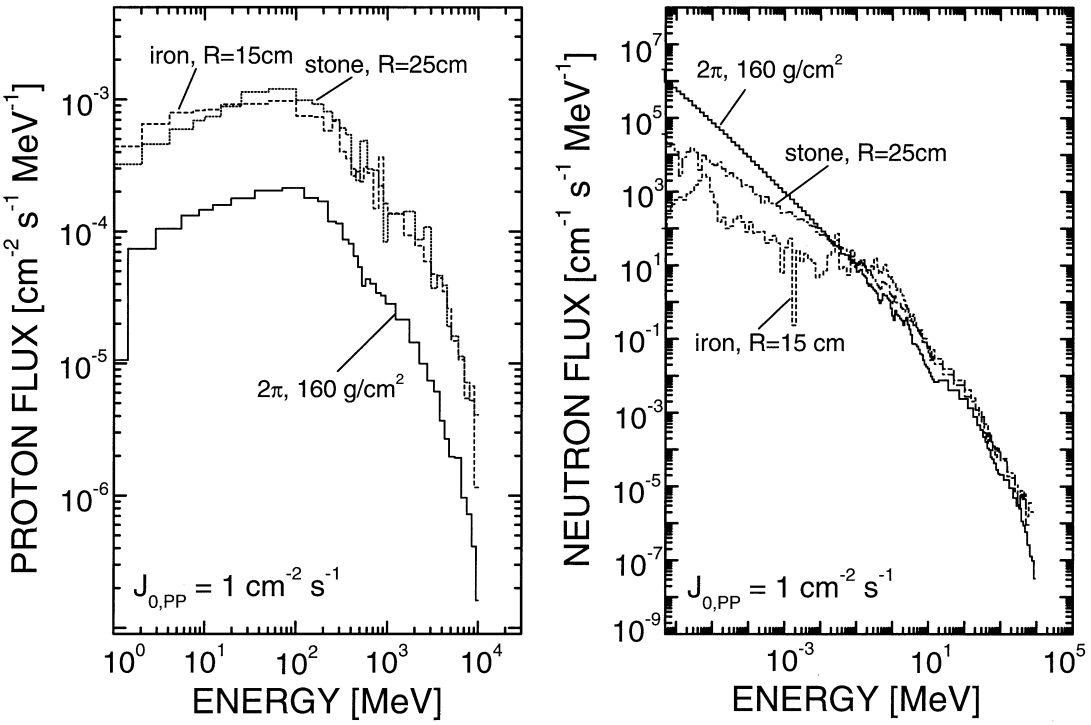

Fig. 1. Differential flux densities of protons (left panel) and neutrons (right panel) at the center of a 15 cm (118 g/cm^2) iron meteoroid, at the center of a 25 cm (75 g/cm^2) stony meteoroid and in lunar surface material at a shielding depth of 160 g/cm^2. The data are obtained by Monte-Carlo-techniques and are normalised to an incoming flux of primary protons of 1 cm^{-2} s^{-1}.

Yin et al. (1992). More information on neutron capture produced isotopic anomalies in lunar samples can be found in the pioneering work by Lingenfelter et al. (1972). For some recent studies of neutron capture isotopes, including isotopic shifts in cadmium, the reader is referred to Sands et al. (2001).

2. MODEL CALCULATIONS

We calculated production rates of cosmogenic nuclides P_j by integrating the depth- and size- dependent spectra of primary and secondary particles with the excitation functions of the relevant nuclear reactions:

$$P_j(M, d, R) = \sum_{i=1}^{N} c_i \frac{N_A}{A_i} \sum_{k=1}^{3} \int_0^{\infty} \sigma_{j,i,k}(E) \times J_k(E, M, d, R) dE \quad (1)$$

where N_A is Avogadro's number, A_i the mass number of the target element i, c_i the abundance of i (g/g), and k is an index for the reaction particle type (primary protons, secondary protons, and secondary neutrons). $\sigma_{j,i,k}(E)$ is the excitation function for the production of nuclide j from target element i by reactions induced by particles of type k. The shielding depth of the sample is d and R is the radius of the irradiated object. E and M are the energy of the reacting particles and the solar modulation parameter, respectively. The model explicitly takes into account only proton- and neutron-induced reactions. We consider primary and secondary galactic α-particles only in an approximate way by multiplying the production rates from protons and neutrons by a factor 1.55 (Leya et al., 2000b). This needs to be done because the cross sections needed for accurate modelling are not yet available. For more details about the model calculations and the α-approximation the reader is referred to Leya et al. (2000a, 2000b).

The particle spectra were derived by following the trajectories of primary GCR-particles and calculating production and transport of secondary particles, both using Monte-Carlo-Techniques. These calculations were done using the HET- (Armstrong and Chandler, 1972, Armstrong et al., 1972) and MORSE-codes (Emmett, 1975) within the HERMES code system (Cloth et al., 1988). To model the production rates for lunar samples we use the particle spectra described by Leya et al. (2001b) and Lange (1994). The production rates in stony meteoroids were modelled using the spectra described by Leya et al. (2000a, 2000b). For iron meteorites we rely on the differential flux densities discussed in detail by Leya (1997). In Figure 1 we show examples of differential flux densities of primary and secondary protons and secondary neutrons at the center of a 15 cm ($\equiv$118 g/cm^2) iron meteoroid, at the center of a 25 cm ($\equiv$75 g/cm^2) stony meteoroid and at a shielding depth of 160 g/cm^2 in a 2π irradiation of the lunar surface.

So far, calculated production rates are normalized to an integral flux density of primary protons with energies $>$ 10 MeV of $J_{0,pp}(E > 10\ \text{MeV}) = 1\ \text{cm}^{-2}\ \text{s}^{-1}$. To compare lunar and meteorite data directly to the model predictions, the production rates calculated using Eqn. 1 have to be multiplied with the integral number of GCR particles ($J_{0,GCR} = 1.55 \times J_{0,pp}$) in the lunar and meteoroid orbits, where the factor of 1.55 is the

Table 1. Target elements and product nuclides considered for capture and spallation reactions.

Extinct nuclide system	Produced isotopes	Reaction pathways
^{53}Mn-^{53}Cr	^{53}Mn, Cr-isotopes	Neutron-capture reactions on Cr-isotopes Spallation reaction on Cr-isotopes Spallation reactions on Fe-isotopes
^{92}Nb-^{92}Zr	^{92}Nb, Zr-isotopes	Neutron-capture reactions on ^{89}Y Neutron-capture reactions on Zr-isotopes Spallation reactions on Zr-isotopes Spallation reactions on ^{93}Nb Spallation reactions on Mo-isotopes
^{98}Tc-^{98}Ru-^{99}Tc-^{99}Ru	^{98}Tc, ^{99}Tc, Mo-isotopes	Neutron-capture reactions on Mo-isotopes Spallation reactions on Mo-isotopes Spallation reactions on Ru-isotopes Spallation reactions on ^{103}Rh
^{182}Hf-^{182}W	^{182}Ta, W-isotopes	Neutron-capture reactions on ^{181}Ta Neutron-capture reactions on W-isotopes Spallation reactions on W-isotopes

All calculated production rates are cumulative, i.e. they include the decay of all radionuclides produced on the corresponding isobar.

α-approximation. For spallation reactions in we use $J_{0,GCR}$ = 4.06 cm^{-2} s^{-1} for stony and iron meteorites (Leya, 1997 and Leya et al., 2000b) and $J_{0,GCR}$ = 4.54 cm^{-2} s^{-1} for lunar rocks (Leya et al., 2001b). Based on GCR-measurements the $J_{0,GCR}$-value in the lunar orbit should be very similar to that in meteoroid orbits. However, different inferred (nominal) $J_{0,GCR}$-values for meteoroid and lunar orbits, respectively, turned out to result from the different GCR-particle spectra used for modelling. The differences have no physical reason. For a comprehensive discussion see Leya et al. (2001b).

For some ill-understood reason, the $J_{0,GCR}$-values that best reproduce the experimental data also differ for spallation reactions and thermal/epithermal neutron capture reactions, respectively. The $J_{0,GCR}$-values for neutron capture reactions in lunar rocks were derived as follows. By adjusting our modelled ^{41}Ca depth profile for the Apollo 15 drill core to experimental data from Nishiizumi et al. (1997) we derived a $J_{0,GCR}$-value for thermal and epithermal neutron capture reactions in the lunar orbit of 2.64 cm^{-2} s^{-1}. Using this value our calculated ^{41}Ca depth profile for lunar samples is in good agreement with earlier modelling by Nishiizumi et al. (1997). However, this value is 46% lower than our earlier estimate (Leya et al., 2000a). The new results for ^{182}Hf-^{182}W given below should therefore replace our earlier data (Leya et al., 2000a). Since for meteorites no measured ^{41}Ca depth profiles exist and therefore no direct adjustment of the modelled results to experimental data is possible, the $J_{0,GCR}$-value for thermal and epithermal neutron capture reactions in meteorites is determined by the requirement to be consistent with the value for lunar samples. We thus divided the $J_{0,GCR}$-value for spallation reactions in meteorites with the $J_{0,GCR}$-value for spallation reactions in lunar samples, and multiplied this ratio with the lunar $J_{0,GCR}$-value for neutron capture reactions, i.e., (4.06/4.54) $\times$ 2.64 = 2.36. Hence, for the model calculations of the neutron capture reactions in meteorites we rely on an integral number of GCR particles of $J_{0,GCR}$= 2.36 cm^{-2} s^{-1}.

The excitation functions for (n,γ)-reactions for energies up to 20 MeV are based on ENDF/B-VI data (Kinsey, 1979). For higher energies the (n,γ)-cross sections are assumed to be zero. For all other reactions the cross sections from the respective reaction threshold up to 260 MeV were calculated on the basis of the Hybrid-Model for preequilibrium reactions (Blann, 1971) using the ALICE-IPPE code (Shubin et al., 1995). For energies above 260 MeV the Hybrid-Model cross sections are assumed to be constant. The total burnout of the target isotopes was calculated using the total reaction cross section in the parameterised version of Tripathi et al. (1997). We correct these data for the inelastic scattering of the projectiles, which is included in the total reaction cross sections but which does not alter the isotopic ratios, using the results from the Hybrid-Model calculations. Table 1 summarises the target elements and product nuclides considered in our study for capture and spallation reactions.

We want to emphasise that production and consumption rates based only on theoretical cross sections may be wrong by more than a factor of 2. In a recent evaluation Michel and Nagel (1997) showed that model calculations for activation yields at intermediate energies on a purely predictive basis may at best have uncertainties of the order of a factor of 2, although the Hybrid-Model version used here (Shubin et al., 1995) is one of the most suitable model codes (Michel and Nagel, 1997). On the other hand, most of the results given in this paper are not significantly affected by these uncertainties, because we will see below that medium and high energy spallation reactions only slightly change the isotopic ratios of interest. For the Hf-W-system, in which the effects are large, the main reaction is ^{181}Ta(n,γ)^{182}Ta(β^-)^{182}W, for which accurate ENDF/B-VI cross sections are available.

3. RESULTS

The modelled GCR-induced isotopic shifts of Cr, Zr, Ru and W as a function of radii, shielding depth, and the chemical composition of the target are available as EXCEL files from the correspondence author.

3.1. Searching for a Proxy of the Projectile Fluence for Each Extinct Nuclide System

The production rates calculated via Eqn. 1 are in units of [g^{-1}s^{-1}]. To quantify the integrated effect, i.e., the total isotopic shift due to cosmic-ray irradiation, the fluence of the relevant particle types has to be known. In the first study of the

^{182}Hf-^{182}W-system, where the GCR-induced shift in ^{182}W is mainly by the thermal neutron capture reaction ^{181}Ta(n,γ)^{182}Ta(β^-)^{182}W, we used as proxy for the dose of thermal and epithermal neutrons the cosmogenic ^{21}Ne and ^{38}Ar exposure ages, because these data are widely available. While this approach gives reliable results for lunar rocks for shielding depths larger than ~200 g/cm^2—at these irradiation depths the ratio Φ_n(thermal + epithermal)/Φ_n(fast) is nearly constant—it overestimates GCR-induced effects by about a factor of 10 for samples which were irradiated at the very top of the lunar regolith, because there the actual flux of thermal and epithermal neutrons is much lower than that derived straightforwardly from cosmogenic ^{21}Ne and ^{38}Ar. For example, the neutron capture rates on ^{181}Ta increase from the surface to the local maximum at ~200 g/cm^2 by more than a factor of 15, whereas the ^{21}Ne production rates only increase by ~50% and peak at lower depths of ~60 g/cm^2. For more detailed discussions about production mechanisms for neutron capture nuclides the reader is referred to Lingenfelter et al. (1972) for lunar rocks and Spergel et al. (1986) for meteorites. Spallation systematics in lunar rocks are discussed in Reedy and Arnold (1972) and Leya et al. (2001b).

In the following, we will deduce improved proxies for the relevant particle fluences for the Hf-W, Mn-Cr, and Nb-Zr systems. Unfortunately, for ^{98}Tc-^{98}Ru and ^{99}Tc-^{99}Ru no appropriate proxy for the projectile fluence could be found. For the ratios that are mainly altered by thermal, epithermal or other low energetic particles (E < ~10 MeV), e.g., ^{182}W/^{184}W and ^{92}Zr/^{90}Zr, we give the GCR-induced shifts as a function of ^{149}Sm/^{150}Sm and ^{157}Gd/^{158}Gd. In contrast, ^{53}Cr/^{52}Cr is mainly altered by medium to high energy spallation reactions on Fe and the dose of the sample can best be estimated via the GCR-induced shift in ^{54}Cr/^{52}Cr.

However, for most samples investigated so far for their isotopic anomalies, no ^{157}Gd/^{158}Gd or ^{149}Sm/^{150}Sm data are available. To roughly estimate the GCR-induced effects we give a relationship between the cosmic-ray exposure age, which can easily be determined via the cosmogenic ^{21}Ne and/or ^{38}Ar, and the GCR induced shifts in ^{157}Gd/^{158}Gd for stony and iron meteorites and for lunar rocks. The determination of exposure ages from cosmogenic ^{21}Ne or ^{38}Ar concentrations is not straightforward because the production rates strongly depend on the shielding depth. For lunar samples this problem can be circumvented by giving 'nominal' ages, which are minimal ages because they are based on maximum production rates. Therefore, in the interests of consistency we rely here also on nominal cosmic-ray exposure ages. Consequently, we assume maximum GCR-induced shifts in ^{157}Gd/^{158}Gd and ^{149}Sm/^{150}Sm, i.e., minimum ^{157}Gd/^{158}Gd and ^{149}Sm/^{150}Sm ratios. The relationships between the minimum ^{157}Gd/^{158}Gd ratio and the nominal cosmic-ray exposure age for stony and iron meteorites and 2π exposure geometries are:

$$Min\left(\frac{^{157}\mathrm{Gd}}{^{158}\mathrm{Gd}}\right)_{2\pi} = 0.63023 - 1.38 \times 10^{-5} \times \mathrm{T_{exp}}$$

$$Min.\left(\frac{^{157}\mathrm{Gd}}{^{158}\mathrm{Gd}}\right)_{stone} = 0.63023 - 3.20 \times 10^{-5} \times \mathrm{T_{exp}} \quad (2)$$

$$Min.\left(\frac{^{157}\mathrm{Gd}}{^{158}\mathrm{Gd}}\right)_{iron} = 0.63023 - 2.78 \times 10^{-7} \times \mathrm{T_{exp}}$$

where *Min.*(^{157}Gd/^{158}Gd) is the minimum ratio expected for any meteoroid radius, 0.63023 the normal isotopic ^{157}Gd/^{158}Gd ratio (Eugster et al., 1970), and T_{exp} is the cosmic-ray exposure age in Myrs. Note that the different multipliers of T_{exp} are due to the "matrix-effect," which causes differences in the thermalised neutron fluence in different materials. With these correlations the cosmic-ray induced shifts given below as a function of ^{157}Gd/^{158}Gd and ^{149}Sm/^{150}Sm can easily be transferred into upper limits for the GCR-induced effects as a function of the more widely available cosmic-ray exposure ages. Note, however, that using the nominal exposure ages results in upper limits for the GCR-induced shifts and that the main improvement of the present version of model calculations is the incorporation of proper proxies for the projectile fluences, which allows an accurate determination of the expected GCR-induced shifts. Considering Eqn. 4 it should be emphasised that the lowering of the ^{157}Gd/^{158}Gd ratio with cosmic-ray exposure is for the same T_{exp} more pronounced in stony meteoroids (4π) than in lunar rocks (2π) simply because the fluence of secondary particles like thermal neutrons is higher if the object is irradiated under 4π conditions compared to a 2π irradiation.

3.2. The ^{182}Hf-^{182}W-System

3.2.1. The ^{182}Hf-^{182}W-system in lunar samples

In Figure 2 the cosmic-ray induced shift ε_{GCR}(^{182}W/^{184}W) is plotted as a function of ^{149}Sm/^{150}Sm (upper abscissa) and ^{157}Gd/^{158}Gd (lower abscissa) for lunar rocks. For the calculations we used Ta/W = 5, which is an average value for lunar samples. Note that ε_{GCR}(^{182}W/^{184}W) linearly correlates with the Ta/W ratio because ^{181}Ta(n,γ)^{182}Ta(β^-)^{182}W is the dominant reaction. Hence, assuming, e.g., Ta/W = 10 would increase the slope of the correlation by a factor of 2 but would not change the narrow correlation between the cosmic-ray shifted ^{182}W/^{184}W and the neutron dose proxies ^{157}Gd/^{158}Gd and ^{149}Sm/^{150}Sm, respectively. For further discussion it is sufficient to approximate the predicted data range given by the model calculations between ε_{GCR}(^{182}W/^{184}W) and ^{149}Sm/^{150}Sm and ^{157}Gd/^{158}Gd, respectively, by linear relationships.

$$\varepsilon_{GCR}\left(\frac{^{182}\mathrm{W}}{^{184}\mathrm{W}}\right)_{2\pi} = -20.30 + 32.21 \times \left(\frac{^{157}\mathrm{Gd}}{^{158}\mathrm{Gd}}\right) + \left(\frac{\mathrm{Ta}}{\mathrm{W}}\right) \times \left\{76.06 - 120.68 \times \left(\frac{^{157}\mathrm{Gd}}{^{158}\mathrm{Gd}}\right)\right\} \quad (3)$$

and:

$$\left(\frac{^{157}\mathrm{Gd}}{^{150}\mathrm{Gd}}\right)_{2\pi} = 0.5639 \times \left(\frac{^{149}\mathrm{Sm}}{^{150}\mathrm{Sm}}\right) - 0.4259 \quad (4)$$

The latter relationship is in reasonable agreement with the experimental data by Hidaka et al. (1999, 2000). Based on Eqn. 3 the GCR-induced effects on ^{182}W/^{184}W in lunar rocks can be calculated without the explicit knowledge of the exposure age and the shielding depth of the sample within an uncertainty of ±30% by measuring ^{157}Gd/^{158}Gd or ^{149}Sm/^{150}Sm in an aliquot. Of the given uncertainty, ~25% is due to the wideness of the modelled relationships (see Fig. 2), which is due to shielding effects, and ~10% is due to the inherent uncertainty in the model calculations. Note that for some samples the relationship between ^{157}Gd/^{158}Gd and ^{149}Sm/^{150}Sm is not well described

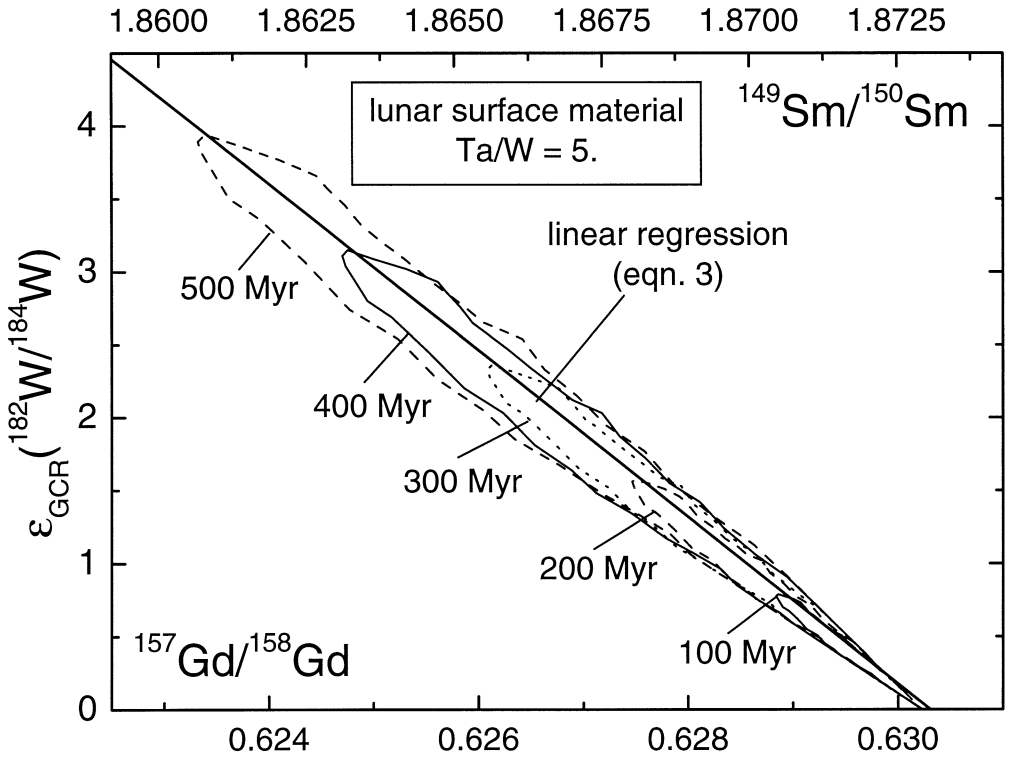

Fig. 2. $\varepsilon_{GCR}(^{182}W/^{184}W)$ as a function of $^{157}Gd/^{158}Gd$ (lower abscissa) and $^{149}Sm/^{150}Sm$ (upper abscissa) for lunar samples with Ta/W = 5 and cosmic-ray exposure ages between 100 Myr and 500 Myr. The plotted solid line is from the linear regression (Eqn. 3). Note that $\varepsilon_{GCR}(^{182}W/^{184}W)$ linearly correlates with the Ta/W ratio because $^{181}Ta(n,\gamma)^{182}Ta(\beta^-)^{182}W$ is the dominant reaction. Hence, assuming, e.g., Ta/W = 10 would increase the slope of the correlation by a factor of 2 but would not change the narrow correlation between the cosmic-ray shifted $^{182}W/^{184}W$ and the neutron fluence proxies $^{157}Gd/^{158}Gd$ and $^{149}Sm/^{150}Sm$.

by Eqn. 4. For samples with high concentrations of elements with large thermal and/or epithermal neutron capture cross sections, e.g., some REE and Fe, the thermal neutron flux can be depressed because either a significant fraction of the neutrons are captured before being thermalised or the neutrons are more rapidly captured at thermal energies (e.g., Lingenfelter et al., 1972). For those samples, $^{149}Sm/^{150}Sm$ is a better proxy for the neutron fluence because the relevant capture resonances in ^{149}Sm and ^{181}Ta are of similar energy. In contrast, the resonance capture in ^{157}Gd is at significantly lower energies. Note that the linear relationships given in this paper are derived by fitting analytical functions to our modelled data. Therefore, in some cases, the nil effect (zero irradiation time) slightly differs from $\varepsilon = 0$ due to the uncertainties ascribed to the rounding of the coefficients deduced for the analytical expressions.

Eqn. 5 and Figure 3 give GCR-induced shifts as a function of $^{157}Gd/^{158}Gd$ (lower abscissa) and $^{149}Sm/^{150}Sm$ (upper abscissa) of the two ratios $^{184}W/^{186}W$ and $^{183}W/^{184}W$, those that are commonly used to correct for instrumental mass fractionation. Using again a simplified linear relationship, which describes the modelled data to within ~25%, we get:

$$\varepsilon_{GCR}\left(\frac{^{184}W}{^{186}W}\right)_{2\pi} = 19.579 - 31.066 \times \left(\frac{^{157}Gd}{^{158}Gd}\right)$$
$$\varepsilon_{GCR}\left(\frac{^{183}W}{^{184}W}\right)_{2\pi} = 15.273 - 24.233 \times \left(\frac{^{157}Gd}{^{158}Gd}\right) \quad (5)$$

Both equations can easily be transferred to the neutron dose proxy $^{149}Sm/^{150}Sm$ with Eqn. 4.

The cosmic-ray effects on the W-isotopic ratios calculated via Eqn. 3 and 5 and using the relationship between $^{157}Gd/^{158}Gd$ and the cosmic-ray exposure age (Eqn. 2) are ~30% lower than our earlier estimates (Leya et al., 2000a). This is only due to the lower $J_{0,GCR}$-value used here. The new results should therefore replace the relationships given in Leya et al. (2000a).

To summarise, by using the isotopic ratios $^{157}Gd/^{158}Gd$ and $^{149}Sm/^{150}Sm$ as proxies for the thermal and epithermal neutron dose, the GCR-induced shifts in $^{182}W/^{184}W$, $^{184}W/^{186}W$, and $^{183}W/^{184}W$ in lunar rocks can be determined within ±30% without the explicit knowledge of the exposure age and the shielding depth of the sample. Therefore, the present version of the model calculations are accurate enough to reliably recognise and correct measured ^{182}Hf-^{182}W-data for GCR-induced effects.

3.2.2. The ^{182}Hf-^{182}W-system in stony and iron meteorites

In Figure 4 the cosmic-ray induced shifts in $\varepsilon_{GCR}(^{182}W/^{184}W)$, $\varepsilon_{GCR}(^{184}W/^{186}W)$, and $\varepsilon_{GCR}(^{183}W/^{184}W)$ are plotted as a function of $^{157}Gd/^{158}Gd$ (lower abscissa) and $^{149}Sm/^{150}Sm$ (upper abscissa) for stony meteorites with radii between 5 cm and 120 cm, respectively. As with lunar rocks the modeled results for stony meteorites in the left hand panel show a

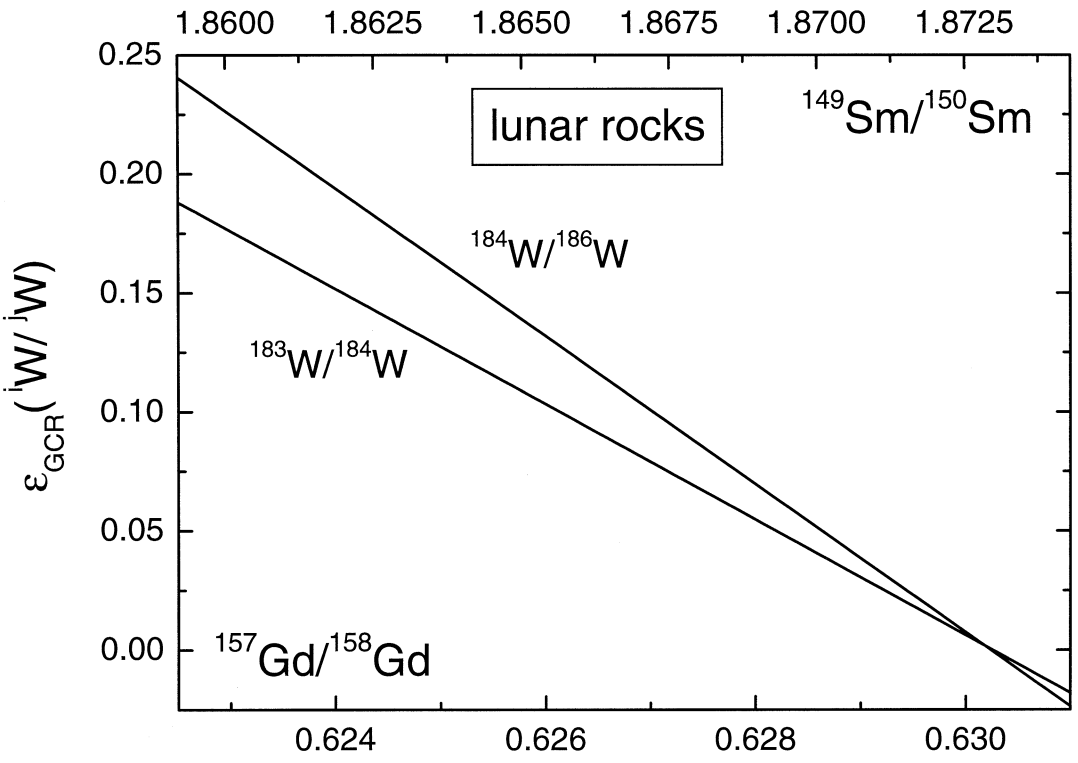

Fig. 3. $\varepsilon_{GCR}(^{183}W/^{184}W)$ and $\varepsilon_{GCR}(^{184}W/^{186}W)$ as a function of $^{157}Gd/^{158}Gd$ (lower abscissa) and $^{149}Sm/^{150}Sm$ (upper abscissa) for lunar samples. The two W-ratios are used for instrumental mass fractionation. If $^{183}W/^{184}W$ is used, the true $\varepsilon(^{182}W/^{184}W)$ becomes slightly smaller than the value obtained by assuming the terrestrial $^{183}W/^{184}W$ value, with $^{186}W/^{184}W$ the true $\varepsilon(^{184}W/^{186}W)$ will become slightly larger. Note that the effects are mostly smaller than present-day analytical uncertainties.

narrow correlation between $\varepsilon_{GCR}(^{182}W/^{184}W)$ and the Gd- and Sm-isotopic ratios. This again allows us to use linear approximations. The following relationships can be used to correct the measured data.

$$\varepsilon_{GCR}\left(\frac{^{182}W}{^{184}W}\right)_{stone} = -22.29 + 35.36 \times \left(\frac{^{157}Gd}{^{158}Gd}\right) + \left(\frac{Ta}{W}\right) \times \left\{83.31 - 132.19 \times \left(\frac{^{157}Gd}{^{158}Gd}\right)\right\}$$

$$\varepsilon_{GCR}\left(\frac{^{184}W}{^{186}W}\right)_{stone} = 20.88 - 33.13 \times \left(\frac{^{157}Gd}{^{158}Gd}\right) \quad (6)$$

$$\varepsilon_{GCR}\left(\frac{^{183}W}{^{184}W}\right)_{stone} = 16.92 - 26.84 \times \left(\frac{^{157}Gd}{^{158}Gd}\right)$$

and

$$\left(\frac{^{157}Gd}{^{158}Gd}\right)_{stone} = 0.5614 \times \left(\frac{^{149}Sm}{^{150}Sm}\right) - 0.4208 \quad (7)$$

We already demonstrated that due to low Ta/W (e.g., 0.2 to 0.75 for Martian meteorites (Lodders, 1998)), and the low exposure ages of only a few million years, the GCR-induced effects on W-isotopes in stony meteorites typically can be neglected (Leya et al., 2000a). Reported W-excesses in Martian meteorites and eucrites therefore are essentially due to the early decay of ^{182}Hf.

For iron meteorites the system becomes simpler because the target element Ta is lacking. Hence, any cosmic-ray effects in iron meteorites are due to isotopic shifts within the W itself (see also Masarik, 1997). The modelled correlations for iron meteorites are:

$$\varepsilon_{GCR}\left(\frac{^{182}W}{^{184}W}\right)_{iron} = -737.68 + 1170.50 \times \left(\frac{^{157}Gd}{^{158}Gd}\right)$$

$$\varepsilon_{GCR}\left(\frac{^{184}W}{^{186}W}\right)_{iron} = 780.87 - 1239.03 \times \left(\frac{^{157}Gd}{^{158}Gd}\right) \quad (8)$$

$$\varepsilon_{GCR}\left(\frac{^{183}W}{^{184}W}\right)_{iron} = 368.43 - 584.59 \times \left(\frac{^{157}Gd}{^{158}Gd}\right)$$

and

$$\left(\frac{^{157}Gd}{^{158}Gd}\right)_{iron} = 0.3330 \times \left(\frac{^{149}Sm}{^{150}Sm}\right) + 0.0068 \quad (9)$$

Assuming a cosmic-ray exposure age of 600 Myr, the minimum $^{157}Gd/^{158}Gd$ in iron meteorites is 0.630065 (Eqn. 2). With Eqn. 8 we can calculate the upper limit for $\varepsilon_{GCR}(^{182}W/^{184}W)$ to be < 0.3, in good agreement with the effect modelled by Masarik for the iron meteorite Toluca (Masarik, 1997).

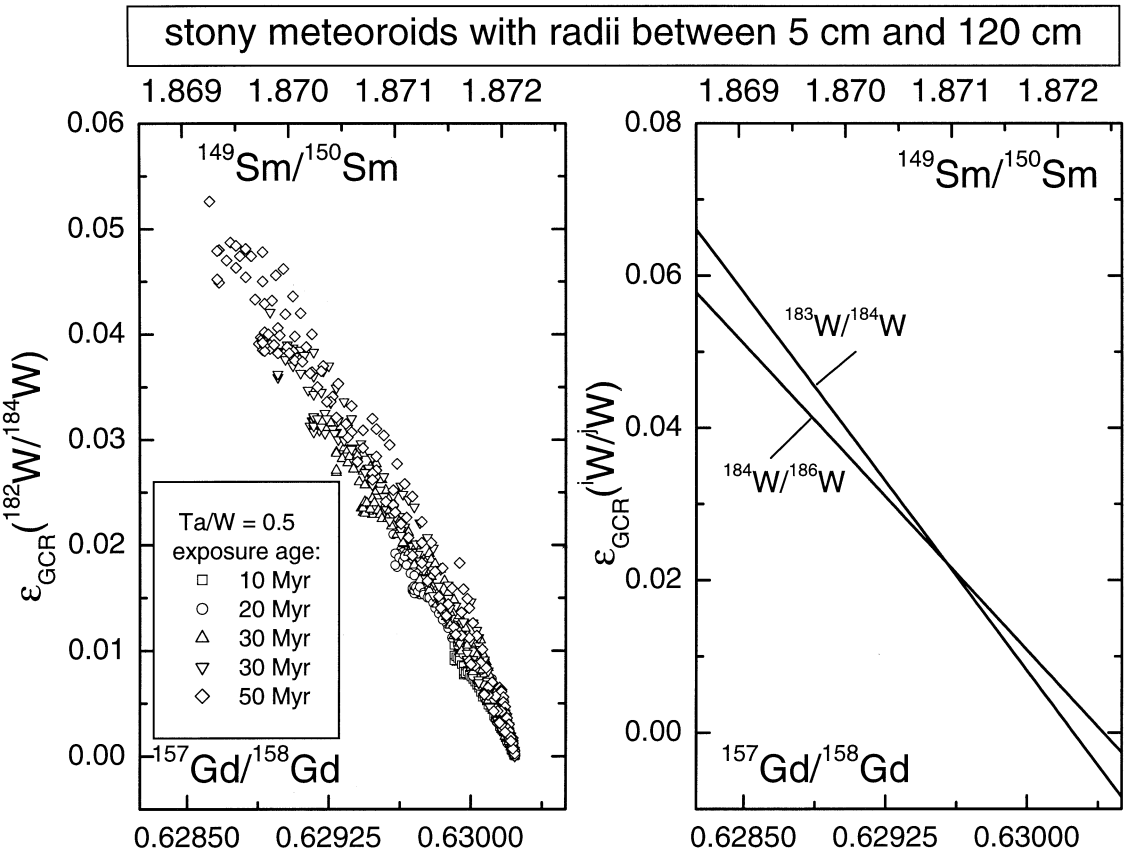

Fig. 4. $\varepsilon_{GCR}(^{182}W/^{184}W)$ as a function of $^{157}Gd/^{158}Gd$ (lower abscissa) and $^{149}Sm/^{150}Sm$ (upper abscissa) for stony meteorites with radii between 5 cm and 120 cm and cosmic-ray exposure ages between 10 Myr and 50 Myr (left panel). The right panel shows the linear correlation between $\varepsilon_{GCR}(^{184}W/^{186}W)$ and $\varepsilon_{GCR}(^{183}W/^{184}W)$ as a function of $^{157}Gd/^{158}Gd$ and $^{149}Sm/^{150}Sm$, respectively. These W-isotopic ratios are used to correct for instrumental mass fractionation. For further discussion see also figure caption 3.

3.3. The ^{53}Mn-^{53}Cr-System

The Cr-isotopic ratios, e.g., $^{53}Cr/^{52}Cr$, are mainly altered by proton- and neutron-induced spallation reactions on Fe. Since the depth dependency of spallation products differ significantly from those produced via thermal and epithermal neutron capture, $^{149}Sm/^{150}Sm$ and $^{157}Gd/^{158}Gd$ cannot be used as proxies for the particle fluence. However, $^{54}Cr/^{52}Cr$ is also routinely measured in ^{53}Mn-^{53}Cr analyses. This ratio is also shifted by spallation reactions and is therefore a suitable proxy for the relevant GCR particle fluence of the sample. Note that the inherent uncertainty of the model calculations for the $^{53}Mn/^{53}Cr$ system is difficult to estimate. From extensive and systematic studies of cross sections calculated using the Hybrid-Model for preequilibrium reactions we expect the absolute cross sections to be accurate only to within a factor of 2. However, cross section ratios, i.e., $^{53}Cr/^{52}Cr$, can be calculated more accurately to within ~50%. Therefore, the modelled shifts in the $^{53}Mn/^{53}Cr$ system should be accurate to within ~50%. The modelled GCR-induced shifts in $^{53}Cr/^{52}Cr$ and $^{54}Cr/^{52}Cr$ as a function of radii, shielding depth, and the Fe/Cr-ratio are available as EXCEL-files from the corresponding author.

3.3.1. The ^{53}Mn-^{53}Cr-system in lunar samples

In Figure 5 we have plotted $\varepsilon_{GCR}(^{53}Cr/^{52}Cr)$ as a function of $\varepsilon_{GCR}(^{54}Cr/^{52}Cr)$ for a 2π exposure geometry with cosmic-ray exposure ages between 100 Myr and 500 Myr and Fe/Cr = 75. The correlation between $\varepsilon_{GCR}(^{53}Cr/^{52}Cr)$ and $\varepsilon_{GCR}(^{54}Cr/^{52}Cr)$ for variable Fe/Cr-ratios deduced from the model predictions can be calculated as:

$$\varepsilon_{GCR}\left(\frac{^{53}Cr}{^{52}Cr}\right)_{2\pi} = \varepsilon_{GCR}\left(\frac{^{54}Cr}{^{52}Cr}\right) \times \left\{0.207 + 1.62 \times e^{-\left(\frac{Fe}{6.74 \times Cr}\right)}\right\} \quad (10)$$

The relationship is an exponential, because isotopic shifts are induced both by spallation of Fe and spallation and neutron capture reactions on Cr; hence even at Fe/Cr = 0 neither $\varepsilon_{GCR}(^{53}Cr/^{52}Cr)$ nor $\varepsilon_{GCR}(^{54}Cr/^{52}Cr)$ become zero. For high Fe/Cr ratios (Fe/Cr > 100) spallation of Fe is the dominant effect while at lower Fe/Cr spallation of Cr and thermal neutron capture reactions within Cr also play a role. Assuming a cosmic-ray exposure age of 500 Myr and Fe/Cr = 75 we obtain an upper limit for $\varepsilon_{GCR}(^{54}Cr/^{52}Cr)$ of < 0.23 (from the EXCEL-file) and, with Eqn. 10, an upper limit for $\varepsilon_{GCR}(^{53}Cr/^{52}Cr)$ of <

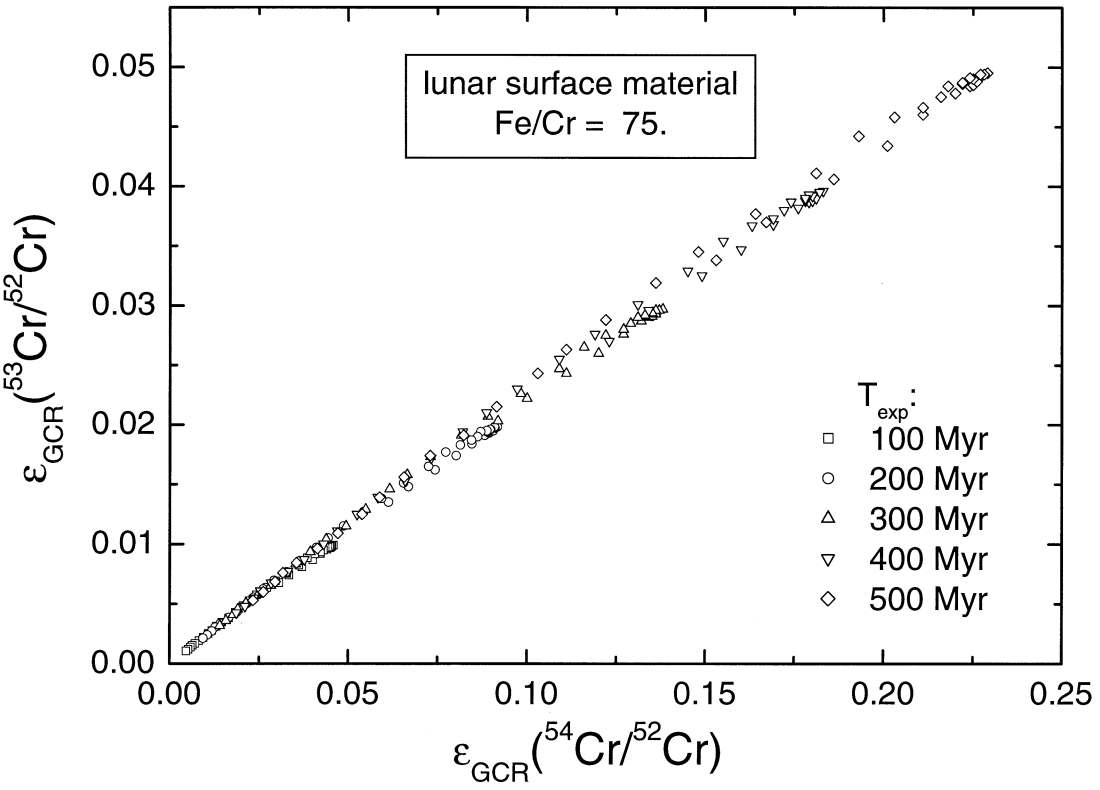

Fig. 5. $\varepsilon_{GCR}(^{53}Cr/^{52}Cr)$ as a function of $\varepsilon_{GCR}(^{54}Cr/^{52}Cr)$ for lunar rocks with cosmic-ray exposure ages between 100 Myr and 500 Myr. The calculations were done using Fe/Cr = 75. Note that the slope is given by the production rate ratio $^{53}Cr/^{54}Cr$, which varies only minor with the Fe/Cr-ratio. Hence, varying the Fe/Cr ratio does not change substantially the slope of the correlation.

0.05. Note that in none of the lunar samples analysed so far for Cr isotopic ratios has an excess of ^{53}Cr been detected (Lugmair and Shukolyukov, 1998). While the absence of GCR-induced effects in lunar rocks is confirmed by the measurements, we will show below that for some iron meteorites considerable GCR-induced isotopic shifts in Cr-isotopes are possible.

3.3.2. The ^{53}Mn-^{53}Cr-system in stony and iron meteorites

For stony meteorites the following relationship holds:

$$\varepsilon_{GCR}\left(\frac{^{53}Cr}{^{52}Cr}\right)_{stone} = 0.178 \times \varepsilon_{GCR}\left(\frac{^{54}Cr}{^{52}Cr}\right) \times \left\{1 - 0.277 \times e^{-\left(\frac{Fe}{94.24 \times Cr}\right)}\right\} \quad (11)$$

Assuming a chondritic sample with Fe/Cr = 75 and a cosmic-ray exposure age of 30 Myr results in an upper limit for $\varepsilon_{GCR}(^{54}Cr/^{52}Cr)$ of 0.035 (from the EXCEL file). With Eqn. 11 we then obtain $\varepsilon_{GCR}(^{53}Cr/^{52}Cr) < 0.006$. In comparison, most values measured so far for stony meteorites are between 0.4 to 0.7 (Lugmair and Shukolyukov, 1998). Therefore, cosmic-ray effects for the Cr isotopic ratios are negligible for stony meteorites.

For iron meteorites the relationship between $\varepsilon_{GCR}(^{53}Cr/^{52}Cr)$ and $\varepsilon_{GCR}(^{54}Cr/^{52}Cr)$ is given by:

$$\varepsilon_{GCR}\left(\frac{^{53}Cr}{^{52}Cr}\right)_{iron} = 0.171 \times \varepsilon_{GCR}\left(\frac{^{54}Cr}{^{52}Cr}\right) \quad (12)$$

Note that this relationship shows no dependence on the Fe/Cr ratio of the sample. Note also that the asymptotic values for Fe/Cr >> 100 differ for lunar rocks and stony and iron meteorites, respectively. The differences between Eqn. 10, 11, and 12 are due to differences in the differential particle spectra (Fig. 1) and the dependence of primary particle attenuation and secondary particles production on the bulk chemistry of the meteorites (for a proper discussion of the 'so called' matrix effect for meteorites see also Masarik and Reedy, 1994 and Leya, 1997).

For samples with high Fe/Cr ratios and long cosmic-ray exposure ages the GCR induced effects are no longer negligible. For two olivine-separates from the pallasite Omolom spallation corrections are necessary (Lugmair and Shukolyukov, 1998). Assuming equal production rates for ^{53}Cr and ^{54}Cr the spallation correction was found to be 0.14 and 0.12 ε. The measured values are 1.1 and 1.2 ε-units (Lugmair and Shukolyukov, 1998). Note that the used production rate ratio $^{53}Cr/^{54}Cr = 1$ is in reasonable agreement with our model predictions (see below).

We end this section with a comparison between our modelled production rate ratio $P(^{53}Cr)/P(^{54}Cr)$ and measured data for iron meteorites. For the model calculations we obtain $P(^{53}Cr)/P(^{54}Cr)$ between 0.9 and 0.7, depending on radius and

shielding depth, the average value being 0.76. This is in good agreement with the value of 0.63 measured for the iron meteorite Grant (Birck and Allègre, 1984) and the value of ~1 given by Shima and Honda (1966). Note that due to the size and matrix effect mentioned above, the ratio P(^{53}Cr)/P(^{54}Cr) in stony meteorites and lunar rocks is 0.79 and 0.91, respectively.

3.4. The ^{92}Nb-^{92}Zr-system

In the ^{92}Nb-^{92}Zr-system the ratio ^{92}Zr/^{90}Zr is mainly altered by neutron capture reactions on Zr isotopes and by the production of ^{92}Zr via the reaction ^{93}Nb(n,2n)^{92}Nb(β^+)^{92}Zr. For all these reactions the ratios ^{149}Sm/^{150}Sm and ^{157}Gd/^{158}Gd serve as reliable proxies for the particle fluence. For modelling the target elements Y, Zr, Nb and Mo were considered. For practical purposes, however, the cosmic-ray induced shift depends only on the Nb/Zr ratio of the sample. We therefore give the ε_{GCR}-values as a function of the cosmic-ray exposure age and the Nb/Zr ratio.

3.4.1. The ^{92}Nb-^{92}Zr-system in lunar samples

For lunar rocks the cosmic-ray induced shift in ^{92}Zr/^{90}Zr as a function of ^{157}Gd/^{158}Gd can be calculated as:

$$\varepsilon_{GCR}\left(\frac{^{92}Zr}{^{90}Zr}\right)_{2\pi} = 0.09190 - 0.14585 \times \left(\frac{^{157}Gd}{^{158}Gd}\right) + \left(\frac{Nb}{Zr}\right) \times \left\{0.05035 - 0.07989 \times \left(\frac{^{157}Gd}{^{158}Gd}\right)\right\} \quad (13)$$

By assuming a cosmic-ray exposure age of 500 Myr and a chondritic Nb/Zr-ratio of 0.065 we obtain a minimum ^{157}Gd/^{158}Gd of 0.6233 (Eqn. 2) and an upper limit for ε_{GCR}(^{92}Zr/^{90}Zr) = 1.1×10^{-3}. The lack of cosmic-ray effects on Zr-isotopes is confirmed by data that reveal no measurable excesses or deficiencies of ^{92}Zr in lunar rocks (Münker et al., 2000).

3.4.2. The ^{92}Nb-^{92}Zr-system in stony and iron meteorites

In Eqn. 14 we give ε_{GCR}(^{92}Zr/^{90}Zr) as a function of ^{157}Gd/^{158}Gd for stony meteorites and variable Nb/Zr-ratios:

$$\varepsilon_{GCR}\left(\frac{^{92}Zr}{^{90}Zr}\right)_{stone} = 0.08180 - 0.12980 \times \left(\frac{^{157}Gd}{^{158}Gd}\right) + \left(\frac{Nb}{Zr}\right) \times \left\{0.01510 - 0.02396 \times \left(\frac{^{157}Gd}{^{158}Gd}\right)\right\} \quad (14)$$

with $\pm\varepsilon$(^{92}Zr/^{90}Zr) for ^{157}Gd/^{158}Gd $>$ 0.6297 (i.e., ^{149}Sm/^{150}Sm $>$ 1.87145) and $+\varepsilon$(^{92}Zr/^{90}Zr) otherwise. Eqn. 14 can easily be transferred to the fluence proxy ^{149}Sm/^{150}Sm with Eqn. 7. For stony meteorites the shifts in Zr isotopes due to cosmic-ray interactions strongly depend on radius and shielding depth. Consequently, for small effects, i.e., ^{157}Gd/^{158}Gd $>$ 0.6297 and ^{149}Sm/^{150}Sm $>$ 1.87145, positive and negative GCR-induced shifts in ^{92}Zr/^{90}Zr are possible. Fortunately, the upper and lower limits given by the model can easily be parameterised. Hence, for ^{157}Gd/^{158}Gd $>$ 0.6297 and ^{149}Sm/^{150}Sm $>$ 1.87145, ε_{GCR}(^{92}Zr/^{90}Zr) given in Eqn. 14 represent the upper and lower limit, respectively, of the possible shift, i.e., excesses and deficiencies are possible. For smaller Gd- and Sm-ratios only positive effects, i.e., excesses, are possible. In Figure 6 are shown ε_{GCR}(^{92}Zr/^{90}Zr) for stony meteoroids with chondritic Y/Zr, Nb/Zr, and Mo/Zr-ratios of 0.3, 0.065, and 0.3, respectively, and radii between 5 cm and 120 cm. The exposure ages are 10, 20, and 30 Myr, respectively. Assuming a chondritic Nb/Zr ratio and a cosmic-ray exposure age of 30 Myr results in an upper limit for the cosmic-ray shifted ^{92}Zr/^{90}Zr of $\pm 1 \times 10^{-4}$ ε-units. Even assuming a Nb/Zr ratio of 10, i.e., 150 times chondritic, and an exposure age of ~100 Myrs, ε_{GCR}(^{92}Zr/^{90}Zr) increases only to $\pm 1.7 \times 10^{-3}$. Thus, the GCR-induced shifts in ε(^{92}Zr/^{90}Zr) in stony meteoroids will not be significant, even for samples with high Nb/Zr ratios and long GCR exposure ages. For comparison, the measured values are claimed by some to be as large as -3ε (Sanloup et al., 2000 and Münker et al., 2000).

For iron meteorites the relationship between ε_{GCR}(^{92}Zr/^{90}Zr) and ^{157}Gd/^{158}Gd for variable Nb/Zr-ratios is given in Eqn. 15. Note that for iron meteorites only positive values for ε_{GCR}(^{92}Zr/^{90}Zr) are possible.

$$\varepsilon_{GCR}\left(\frac{^{92}Zr}{^{90}Zr}\right)_{iron} = 5.2755 - 8.3708 \times \left(\frac{^{157}Gd}{^{158}Gd}\right) + \left(\frac{Nb}{Zr}\right) \times \left\{9.5160 - 15.0992 \times \left(\frac{^{157}Gd}{^{158}Gd}\right)\right\} \quad (15)$$

For a silicate inclusion with chondritic Nb/Zr, which was irradiated for ~600 Myrs within an iron meteorite, ε_{GCR}(^{92}Zr/^{90}Zr) is 3×10^{-4}, significantly smaller than present day analytical precision.

To summarise, the cosmic-ray induced shifts in ^{92}Zr/^{90}Zr in lunar rocks and stony and iron meteorites are significantly smaller than present day analytical precision. Therefore, the measured isotopic shifts in meteorites (Münker et al., 2000, Sanloup et al., 2000 and Schönbächler et al., 2001) confirm the former existence of the now extinct ^{92}Nb.

3.5. The ^{98,99}Tc-^{98,99}Ru-system

The Tc-Ru-system has the great advantage to provide time information using two short-lived nuclides, ^{98}Tc and ^{99}Tc. However, estimating the GCR induced effects on Ru-isotopes is difficult because various production pathways from Mo and Rh must be considered besides the isotopic shifts within Ru itself. Unfortunately, the GCR-induced shifts in ^{98}Ru/^{96}Ru and ^{99}Ru/^{96}Ru show no correlation with ^{157}Gd/^{158}Gd, ^{149}Sm/^{150}Sm or with any GCR-induced shifts within the Ru itself, e.g., ^{100}Ru/^{96}Ru or ^{101}Ru/^{96}Ru. Therefore, giving a proper projectile dose proxy is impossible for the Tc-Ru-system. For modelling we considered the target elements Mo, Ru, and Rh. However, the GCR-induced shifts depend to only a very small degree on the Mo-concentrations. Therefore, giving ε_{GCR}(^{98}Ru/^{96}Ru) and ε_{GCR}(^{99}Ru/^{96}Ru) as a function of Rh/Ru-ratio and the cosmic-ray exposure age is adequate.

In lunar rocks as well as in stony and iron meteorites ε_{GCR}(^{98}Ru/^{96}Ru) is > 0 for all radii and shielding depths. We therefore give in Eqn. 16 and 18 the dependence of the upper limit $\varepsilon_{GCR,MAX}$(^{98}Ru/^{96}Ru) on the Rh/Ru-ratio and the cosmic-ray exposure age. The situation is different for ε_{GCR}(^{99}Ru/

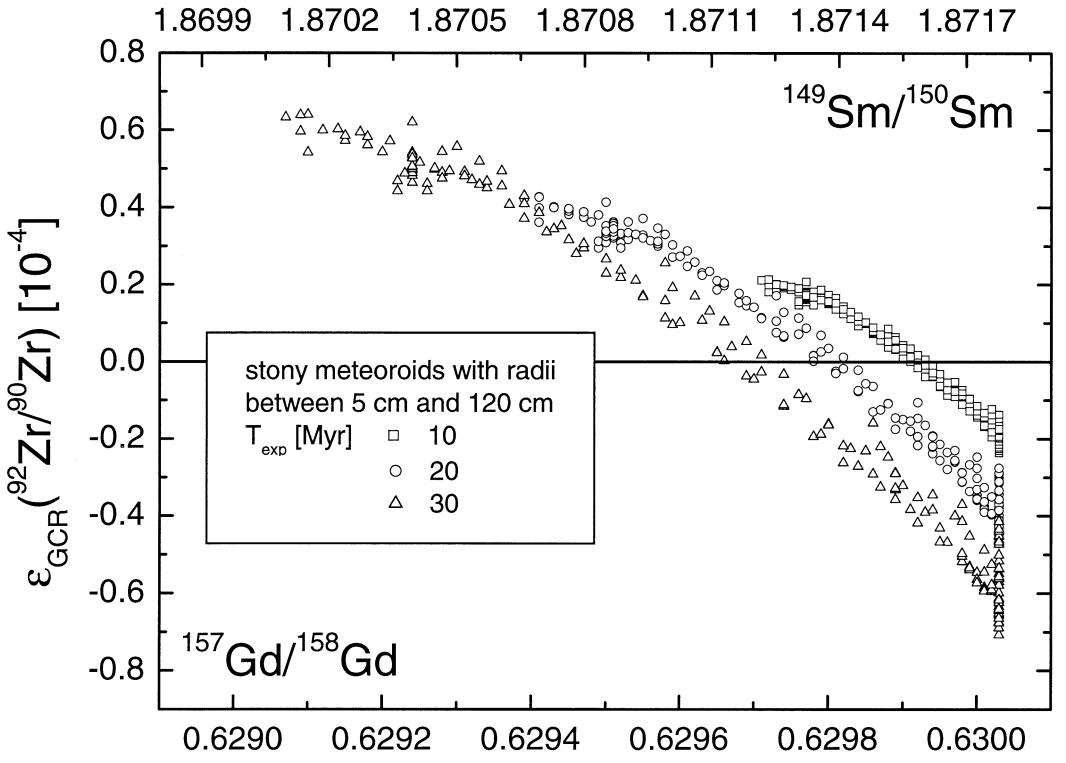

Fig. 6. $\varepsilon_{GCR}(^{92}Zr/^{90}Zr)$ in $[10^{-4}\times Myr^{-1}]$ as a function of $^{157}Gd/^{158}Gd$ (lower abscissa) and $^{149}Sm/^{150}Sm$ (upper abscissa) for stony meteoroids with radii between 5 cm and 120 cm and cosmic-ray exposure ages between 10 Myr and 30 Myr.

^{96}Ru) because this ratio is positive for small meteorites ($R < 25$ cm) and negative for objects with radii > 25 cm (like the Moon). In Eqn. 17 and 19 we therefore give the maximum negative values $\varepsilon_{GCR,lower}(^{99}Ru/^{96}Ru)$ for lunar rocks and stony and iron meteorites and the maximum positive values $\varepsilon_{GCR,upper}(^{99}Ru/^{96}Ru)$ for small meteorites.

3.5.1. The ^{98}Tc-^{98}Ru- and ^{99}Tc-^{99}Ru-system in lunar samples

In Eqn. 16 we give the maximum positive GCR-induced shifts in $^{96}Ru/^{96}Ru$ as a function of the Rh/Ru-ratio and the cosmic-ray exposure age [Myr]:

$$\varepsilon_{GCR,MAX}\left(\frac{^{98}Ru}{^{96}Ru}\right)_{2\pi} = \left\{1.03\times10^{-5} + 4.15\times10^{-6} \times\left(\frac{Rh}{Ru}\right)\right\}\times T_{exp} \quad (16)$$

Assuming a Rh/Ru-ratio of $\sim$0.2 and a cosmic-ray exposure age of 500 Myr results in $\varepsilon_{GCR,MAX}(^{98}Ru/^{96}Ru)$ of 5.5×10^{-3}, smaller than present day analytical precision. Hence, with present day analytical uncertainties the cosmic-ray induced shifts in $^{98}Ru/^{96}Ru$ expected in lunar rocks are negligible. The maximum negative effect in $^{99}Ru/^{96}Ru$ for lunar rocks can be calculated via:

$$\varepsilon_{GCR,lower}\left(\frac{^{99}Ru}{^{96}Ru}\right)_{2\pi} = \left\{-9.35\times10^{-5} + 8.68\times10^{-7} \times\left(\frac{Rh}{Ru}\right)\right\}\times T_{exp} \quad (17)$$

Assuming again Rh/Ru $\sim$0.2 and 500 Myr exposure age results in a cosmic-ray induced shift of smaller than -4.67×10^{-2}.

To summarise, the GCR-induced shifts in $^{98}Ru/^{96}Ru$ and $^{99}Ru/^{96}Ru$ in lunar rocks can be neglected assuming typical cosmic-ray exposure ages of less than 500 Myr and similar to chondritic Rh/Ru-ratios. Even assuming a Rh/Ru ratio 100 times chondritic increases $\varepsilon_{GCR}(^{98}Ru/^{96}Ru)$ to only 0.05 and $\varepsilon_{GCR}(^{99}Ru/^{96}Ru)$ to only -0.04.

3.5.2. The ^{98}Tc-^{98}Ru and ^{99}Tc-^{99}Ru-system in stony and iron meteorites

Figure 7 (left panel) shows our modeled $\varepsilon_{GCR}(^{98}Ru/^{96}Ru)$ $[10^{-6}$ ε/Myr] as a function of radius and shielding depth for stony meteorites with radii between 5 cm and 120 cm and chondritic Rh/Ru-ratios. Based on these data we can deduce the relationship between $\varepsilon_{GCR,MAX}(^{98}Ru/^{96}Ru)$, the Rh/Ru-ratio and the exposure ages [Myr] for stony and iron meteorites:

$$\varepsilon_{GCR,MAX}\left(\frac{^{98}Ru}{^{96}Ru}\right)_{stone} = \left\{2.36\times10^{-6} + 1.42 + 10^{-6} \times\left(\frac{Rh}{Ru}\right)\right\}\times T_{exp} \quad (18)$$

$$\varepsilon_{GCR,MAX}\left(\frac{^{98}Ru}{^{96}Ru}\right)_{iron} = \left\{3.00\times10^{-5} + 1.76 + 10^{-5} \times\left(\frac{Rh}{Ru}\right)\right\}\times T_{exp}$$

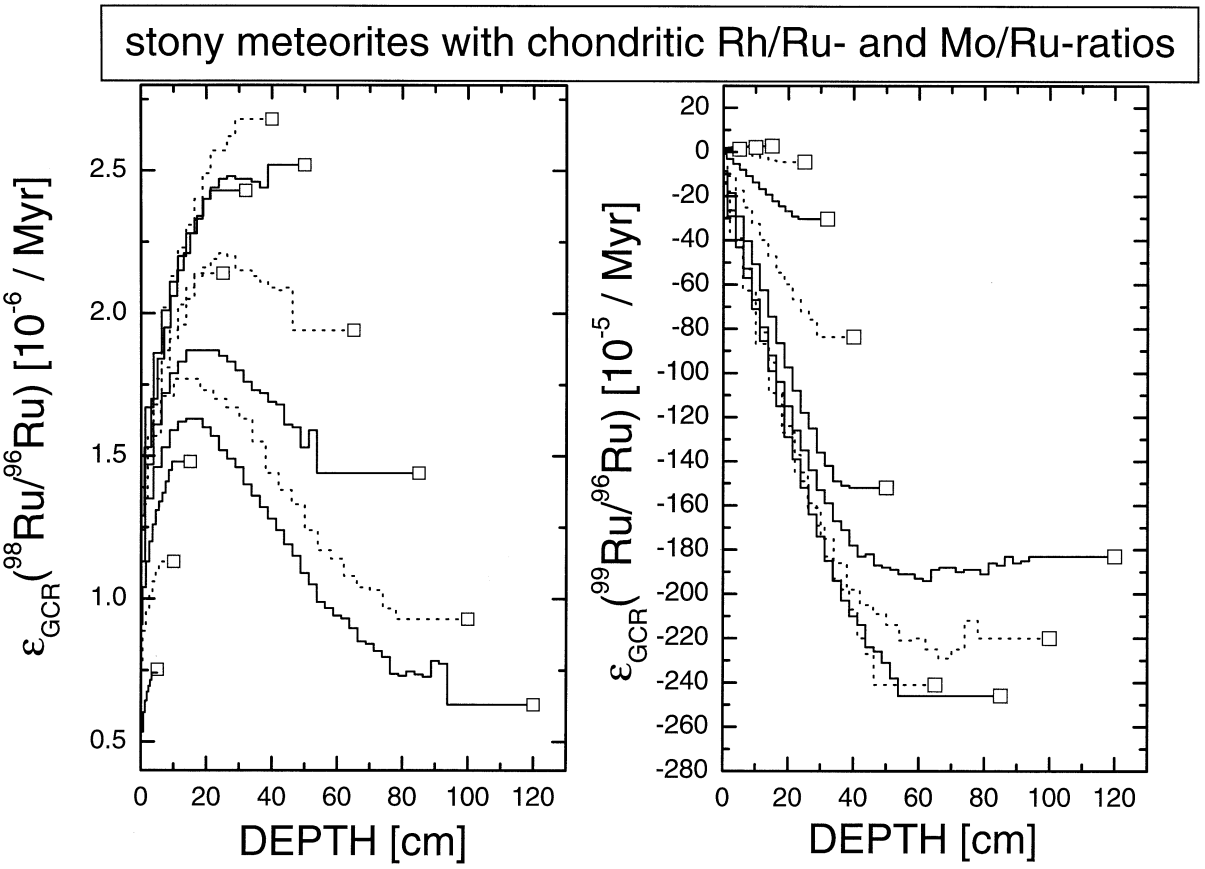

Fig. 7. $\varepsilon_{GCR}(^{98}Ru/^{96}Ru)$ and $\varepsilon_{GCR}(^{99}Ru/^{96}Ru)$ as a function of radius and shielding depth for stony meteoroids with radii between 5 cm and 120 cm. The open boxes indicate the centers of the meteoroids.

Assuming a chondritic Rh/Ru-ratio and exposure ages of 50 Myr and 600 Myr for stony and iron meteorites, respectively, results in a cosmic-ray induced shift of less than 1.5×10^{-3} ε and 0.02 ε for stony and iron meteorites, respectively. Both effects are much smaller than present day analytical precision and can therefore be neglected.

The right panel of Figure 7 shows $\varepsilon_{GCR}(^{99}Ru/^{96}Ru)$ [10^{-5} ε/Myr] as a function of radius and shielding depth for stony meteorites with chondritic Rh/Ru-ratios and radii between 5 cm and 120 cm. From these data it can be seen that the sign of the cosmic-ray shift depends on the size of the meteorites. While $\varepsilon_{GCR}(^{99}Ru/^{96}Ru)$ is positive in small objects ($R < 25$ cm) it becomes negative for objects with radii > 25 cm. We therefore give for stony meteorites in Eqn. 19 the relationships between the maximum positive value $\varepsilon_{GCR,upper}(^{99}Ru/^{96}Ru)$ and the maximum negative value $\varepsilon_{GCR,lower}(^{99}Ru/^{96}Ru)$ as a function of the Rh/Ru-ratio and the cosmic-ray exposure age [Myr]. Note that the maximum negative effect on $^{99}Ru/^{96}Ru$ shows no dependence on the Rh/Ru-ratio for both types of meteorites.

$$\varepsilon_{GCR,upper}\left(\frac{^{99}Ru}{^{96}Ru}\right)_{stone} = \left\{2.34 \times 10^{-6} + 1.39 \times 10^{-6} \times \left(\frac{Rh}{Ru}\right)\right\} \times T_{exp}$$

and (19)

$$\varepsilon_{GCR,lower}\left(\frac{^{99}Ru}{^{96}Ru}\right)_{stone} = -2.45 \times 10^{-4} \times T_{exp}$$

For iron meteorites the relationships are:

$$\varepsilon_{GCR,upper}\left(\frac{^{99}Ru}{^{96}Ru}\right)_{iron} = \left\{4.52 \times 10^{-6} + 2.32 \times 10^{-6} \times \left(\frac{Rh}{Ru}\right)\right\} \times T_{exp}$$

and (20)

$$\varepsilon_{GCR,lower}\left(\frac{^{99}Ru}{^{96}Ru}\right)_{iron} = -7.52 \times 10^{-5} \times T_{exp}$$

With a chondritic Rh/Ru-ratio of 0.2 and cosmic-ray exposure ages of 50 Myr and 600 Myr for stony and iron meteorites the maximum positive effects for $^{99}Ru/^{96}Ru$ are 1.3×10^{-4} ε and 3.0×10^{-3} ε, respectively. The maximum negative effects are -1.2×10^{-2} ε and -4.5×10^{-2} ε, respectively. Even assuming a Rh/Ru ratio of 20, i.e., 100 times chondritic, increases the maximum positive value only to 1.5×10^{-3} and 3.1×10^{-2}, still much smaller than present day analytical precision.

4. CONCLUSIONS

We present new model calculations for the correction of cosmic-ray induced effects on extinct nuclide systems. For the Hf-W-system we give the GCR-induced shifts for lunar rocks and stony and iron meteorites as a function of the Ta/W-ratio and the neutron fluence. The latter can best be estimated via the $^{157}Gd/^{158}Gd$ and $^{149}Sm/^{150}Sm$ ratios in the sample. The measured isotopic shifts in $^{182}W/^{184}W$ can be corrected for their cosmogenic contributions with an uncertainty of $<30\%$ without the knowledge of the shielding depth of the sample and the cosmic-ray exposure age. Hence, the problem of an overestimation of the GCR-induced effects by the model, which compromised so far an accurate correction of the measured isotopic ratios (Leya et al., 2000a), no longer exist.

In addition we present new model results for the cosmic-ray induced shifts in ^{53}Mn-^{53}Cr for stony and iron meteorites and lunar rocks. The predicted absence of GCR-induced effects in lunar rocks, $\varepsilon_{GCR}(^{53}Cr/^{52}Cr) < 0.05$ for samples with chondritic Fe/Cr and 500 Myr exposure age, is confirmed by experimental data, which show no detectable ^{53}Cr excess. For stony meteorites $\varepsilon_{GCR}(^{53}Cr/^{52}Cr)$ typically is smaller than present day analytical precision and therefore can be neglected. In contrast, for at least two olivine samples from within an iron meteorite the GCR-induced shift in $^{53}Cr/^{52}Cr$ accounts for up to 10% of the measured value (Lugmair and Shukolyukov, 1998). Therefore a reliable correction is necessary. We demonstrate that a correction is possible and accurate via the measured $\varepsilon_{GCR}(^{54}Cr/^{52}Cr)$ in the sample.

For the ^{92}Nb-^{92}Zr-system the GCR induced effects in $^{92}Zr/^{90}Zr$ typically can be neglected. Even with an extremely high Nb/Zr-ratio of 150 times chondritic $\varepsilon_{GCR}(^{92}Zr/^{90}Zr)$ typically is $<3 \times 10^{-4}$, which is far beyond analytical precisions. However, the GCR-induced shifts in $^{92}Zr/^{90}Zr$ correlate with $^{157}Gd/^{158}Gd$ and $^{149}Sm/^{150}Sm$ and an accurate correction of the measured data would be possible if required.

Also the cosmic-ray induced shifts in $^{98}Ru/^{96}Ru$ and $^{99}Ru/^{96}Ru$ are negligible. Therefore, the experimental data need no correction and the problem that neither $\varepsilon_{GCR}(^{98}Ru/^{96}Ru)$ nor $\varepsilon_{GCR}(^{99}Ru/^{96}Ru)$ correlate with $^{157}Gd/^{158}Gd$, $^{149}Sm/^{150}Sm$ or any cosmic-ray altered Ru-isotopic ratio is of no practical concern. We nevertheless present maximum positive and negative effects for $\varepsilon_{GCR}(^{98}Ru/^{96}Ru)$ and $\varepsilon_{GCR}(^{99}Ru/^{96}Ru)$ as a function of the cosmic-ray exposure age and the Rh/Ru-ratio of the sample.

To summarise, the GCR-induced effects in the extinct nuclide systems ^{53}Mn-^{53}Cr, ^{92}Nb-^{92}Zr ^{98}Tc-^{99}Tc-^{98}Ru-^{99}Ru and ^{182}Hf-^{182}W were calculated. Significant effects are predicted for the ^{182}Hf-^{182}W-system, but they can readily be corrected via $^{157}Gd/^{158}Gd$ and/or $^{149}Sm/^{150}Sm$. For all other systems the GCR-induced effects are only very minor. The only exception to this is the ^{53}Mn-^{53}Cr-system for which detectable shifts by cosmic-ray interactions may be possible. However, the new model calculations offer the possibility to correct for these effects via the cosmic-ray altered $^{54}Cr/^{52}Cr$ ratio.

Acknowledgments—This work was supported by the Swiss National Science Foundation. The suggestions and comments by the referees J. Masarik, L. Nyquist and R.C. Reedy, and the associate editor U. Ott are appreciated.

Associate editor: U. Ott

REFERENCES

Armstrong T. W. and Chandler K. C. (1972) HETC—A high energy transport code. *Nucl. Sci. Engin.* **49,** 110.

Armstrong T. W., Alsmiller R. G. Jr., Chandler K. C., and Bishop B. L. (1972) Monte Carlo calculations of high-energy nuclear-meson cascades and comparisons with experiment. *Nucl. Sci. Eng.* **49,** 82–92.

Birck J. L., Allègre C. J. (1984) Isotopes produced by galactic cosmic rays in iron meteorites. In *Isotopic Ratios in the Solar System,* (Centre National D'Etudes Spatiales). Cepadues-Editions, Paris. 21–25.

Birck J. L. and Allègre C. J. (1988) Manganese chromium isotope systematics and the development of the early solar system. *Nature* **331,** 579–584.

Blann M. (1971) Hybrid model for pre-equilibrium decay in nuclear reactions. *Phys. Rev. Lett.* **27,** 337–340.

Cloth P., Filges D., Neef R. D., Sterzenbach G., Reul C., Armstrong T. W., Colborn B. L., Anders B., Brückmann H. (1988) HERMES—High Energy Radiation Monte-Carlo Elaborate System, Juelich, Juel-2203.

Emmett M. B. (1975) The MORSE Monte Carlo radiation code system. Oak Ridge National Laboratory ORNL-4942.

Eugster O., Tera F., Burnett D. S., and Wasserburg G. J. (1970) The isotopic composition of Gd and the neutron capture effects in samples from Apollo 11. *Earth Planet. Sci. Lett.* **8,** 20–30.

Goswami J. N. (1998) Short-lived nuclides in the early solar system. *Proc. Indian Acad. Sci. (Earth Planet. Sci).* **107,** 401–411.

Halliday A. N., Rehkämper M., Lee D.-C., and Yi W. (1996) Early evolution of the Earth and the Moon: New constraints from Hf-W isotope geochemistry. *Earth Planet. Sci. Lett.* **142,** 75–89.

Harper C. L. Jr (1996) Evidence for ^{92g}Nb in the early solar system and evaluation of a new p-process cosmochronometer from $^{92}Nb/^{92}Mo$. *Astrophys. J.* **466,** 437–456.

Harper C. L. Jr., Völkening J., Heumann K. G., Shih C-Y., and Wiesmann H. (1991) ^{182}Hf-^{182}W: New cosmochronometric constraints on terrestrial accretion, core formation, the astrophysical site of the r-process, and the origin of the solar system. *Lunar Planet. Sci.* **XXII,** 515–516 Lunar Planet. Inst., Houston (abstr.).

Hidaka H., Ebihara M., and Yoneda S. (1999) High fluences of neutrons determined from Sm and Gd isotopic compositions in aubrites. *Earth. Planet. Sci. Lett.* **173,** 41–51.

Hidaka H., Ebihara M., and Yoneda S. (2000) Isotopic study of neutron capture effects on Sm and Gd in chondrites. *Earth Planet. Sci. Lett.* **180,** 29–37.

Kinsey R. (1979) ENDF-102, Data Formats and Procedures for the Evaluated Nuclear Data File ENDF.

Lange H.-J. (1994) Über die Wechselwirkung der galaktischen kosmischen Teilchenstrahlung mit extraterrestrischer Materie, Ph.D. thesis, Univ. Hannover.

Lee D.-C., Halliday A. N., Leya I., and Wieler R. (2001) Cosmogenic tungsten on the Moon. *Meteor. Planet. Sci.* **36,** A111 (abstr.).

Leya I. (1997) Modellrechnungen zur Beschreibung der Wechselwirkungen galaktischer kosmischer Teilchenstrahlung mit Stein und Eisenmeteoroiden, Ph.D-thesis, Univ. Hannover.

Leya I., Wieler R., and Halliday A. N. (2000a) Cosmic-ray production of tungsten isotopes in lunar samples and meteorites and its implications for Hf-W cosmochemistry. *Earth Planet. Sci. Lett.* **175,** 1–12.

Leya I., Lange H.-J., Neumann S., Wieler R., and Michel R. (2000b) The production of cosmogenic nuclides in stony meteoroids by galactic cosmic-ray particles. *Meteor. Planet. Sci.* **35,** 259–286.

Leya I., Wieler R., and Halliday A. N. (2001a) The influence of cosmic-ray production on extinct nuclide systems. New results from improved model calculations. *Lunar Planet. Sci.* **XXXII** Lunar Planet. Inst., Houston. #1521 (abstr.).

Leya I., Neumann S., Wieler R., and Michel R. (2001b) The production of cosmogenic nuclides by galactic cosmic-ray particles for 2π exposure geometries. *Meteor. Planet. Sci.* **36,** 1547–1561.

Lingenfelter R. E., Canfield E. H., and Hampel V. E. (1972) The lunar neutron flux revisited. *Earth Planet. Sci. Lett.* **16,** 355–369.

Lodders K. (1998) A survey of shergottite, nakhlite and chassigny meteorites whole rock compositions. *Meteor. Planet. Sci.* **33,** 183–190.

Lugmair G. W. and Shukolyukov A. (1998) Early solar system timescales according to ^{53}Mn-^{53}Cr systematics. *Geochim. Cosmochim. Acta* **62,** 2863–2886.

Masarik J. and Reedy R. C. (1994) Effects of bulk composition on nuclide production processes in meteorites. *Geochim. Cosmochim. Acta* **58,** 5307–5317.

Masarik J. (1997) Contribution of neutron-capture reactions to observed tungsten isotopic ratios. *Earth. Planet. Sci. Lett.* **152,** 181–185.

Michel R., Nagel P. (1997) International Codes and Model comparison for Intermediate Energy Activation Yield, NEA Report, NSC/DOC.(97)1.

Münker C., Weyer S., Mezger K., Rehkämper M., Wombacher F., and Bischoff A. (2000) Nb-92-Zr-92 and the early differentiation history of planetary bodies. *Science* **289,** 1538–1542.

Nishiizumi K., Fink D., Klein J., Middleton R., Masarik J., Reedy R. C., and Arnold J. R. (1997) Depth profile of ^{41}Ca in an Apollo 15 drill core and the low-energy neutron flux in the Moon. *Earth Planet. Sci. Lett.* **148,** 545–552.

Podosek F. A., Ott U., Brannon J. C., Neal C. R., Bernatowicz T. J., Swan P., and Mahan E. (1997) Thoroughly anomalous chromium in Orgueil. *Meteor. Planet. Sci.* **32,** 617–627.

Poths H., Schmitt-Strecker S., and Begemann F. (1987) On the isotopic composition of ruthenium in the Allende and Leoville carbonaceous chondrites. *Geochim. Cosmochim. Acta* **51,** 1143–1149.

Reedy R. C. and Arnold J. R. (1972) Interaction of solar and galactic cosmic-ray particles with the Moon. *J. Geophys. Res.* **77,** 537–555.

Reedy RC. (1980). Silver isotopic anomalies in iron meteorites: cosmic-ray production and other possible sources. *Proc. 11th Lunar Planet. Sci. Conf.*, 1169–1178.

Sands D. G., DeLaeter J. R., and Rosman K. J. R. (2001) Measurements of neutron capture effects on Cd, Sm and Gd in lunar samples with implications for the neutron energy spectrum. *Earth Planet. Sci. Lett.* **186,** 335–346.

Sanloup C., Blichert-Toft J., Télouk P., Gillet P., and Albarède F. (2000) Zr isotope anomalies in chondrites and the presence of ^{92}Nb in the early solar system. *Earth Planet. Sci. Lett.* **184,** 75–81.

Schönbächler M., Rehkämper M., Halliday A. N., Lee D.-C., Zanda B., Bourot-Denise M., Hattendorf B., and Günther D. (2001) The initial ^{92}Nb/^{93}. Nb of the solar system. *Meteor. Planet. Sci.* **36,** A184–A185 (abstr.).

Shima M. and Honda M. (1966) Distribution of spallation produced chromium between alloys in iron meteorites. *Earth Planet. Sci. Lett.* **1,** 65–74.

Shubin Y. N., Lunev V. P., Konobeyev A. Y., Dityuk A. I. (1995) Computer Code ALICE-IPPE, IAEA, INDC.(CCP)-385, Vienna, Austria.

Spergel M. S., Reedy R. C., Lazareth O. W., Levy P. W., Slatest L. A. (1986) Cosmogenic neutron-capture-produced nuclides in stony meteorites. *Proc. 16th Lunar Planet. Sci. Conf.*, 483–494.

Tripathi R. K., Cucinotta A., Wilson J. W. (1997) Universal Parameterisation of Absorption Cross Sections. NASA Technical Paper. 3621:NASA, Virginia, USA.

Yin Q., Jagoutz E., and Wänke H. (1992) Re-search for extinct ^{99}Tc and ^{98}Tc in the early solar system. *Meteor. Planet. Sci.* **27,** A310 (abstr.).